Cross-Track Infrared Sounder FPMA Performance

S. Masterjohn , A.I. D'Souza, L.C. Dawson, P. Dolan
Boeing Sensor Products, 3370 Miraloma Avenue, Anaheim, CA 92803

P.S. Wijewarnasuriya
Rockwell Scientific Company, 1049 Camino Dos Rios, Thousand Oaks, CA 91360

J. Ehlert
ITT Aerospace/Communications Division, Ft. Wayne, IN

ABSTRACT

The Cross-track Infrared Sounder (CrIS) is one of many instruments that comprise the National Polar-orbiting Operational Environmental Satellite System (NPOESS). The CrIS instrument consists of a Michelson interferometer infrared sounder that is sensitive to wavelengths between 3.5 and 16 microns. This spectral band is achieved by using three separate Focal Plane Module Assemblies (FPMAs) referred to as the Short Wave Infrared module (SWIR, $\lambda_c \sim 5$ µm at 98K), the Mid Wave Infrared module (MWIR, $\lambda_c \sim 9$ µm at 98K), and the Long Wave Infrared module (LWIR, $\lambda_c \sim 16$ µm at 81K). The CrIS instrument measures the earth radiances at high spectral resolution, using the data to provide pressure, temperature and moisture profiles of the atmosphere. The CrIS instrument will help improve both global and regional predictions of weather patterns, storm tracks, and precipitation. The CrIS program selected the use of photovoltaic (PV) detectors for all three spectral bands. PV technology outperforms photoconductive detectors in terms of high sensitivity and linearity. Each FPMA consists of a 3x3 detector-matrix of 9 fields of view (FOV). Each detector is 1,000um in diameter and has its own cold preamplifier, warm post amplifier and high pass filter. This paper describes the performance for all three modules that together form the CrIS Engineering Development Unit 2 (EDU2) Detector Preamp Assembly (DPM).

Molecular Beam Epitaxy (MBE) is used to grow the appropriate bandgap n-type $Hg_{1-x}Cd_xTe$ on lattice matched CdZnTe. SWIR, MWIR and LWIR 1000 µm diameter detectors have been manufactured using the Lateral Collection Diode (LCD) architecture[1-5]. Custom pre-amplifiers have been designed to interface with the large SWIR, MWIR and LWIR detectors. The operating temperature is above 78K, permitting the use of passive radiators in spacecraft to cool the detectors. Recently, all three FPMAs were completed and tested. The tests performed on each module are listed in Table 1.

Table 1

FPMA Testing
1. Response Nonlinearity
2. Noise Spectral Density
3. D* Calculation
4. Ambient Power Dissipation
5. Dynamic Range

Prior to building the FPMAs, the candidate detectors were screened for properties consistent with those listed in Table 2[6]. The D* values in Table B are calculated at the CrIS program peak wavelength specified for each spectral band.

Table 2

	SWIR	MWIR	LWIR
Operating Temperature (K)	98	98	81
λ_c in µm	5.02	9.89	15.9
R_oA_{opt} in ohm-cm^2	9.0×10^{6}	1.0×10^{2}	1.5×10^{0}
I_d at V_d = -0.1 V	1.0×10^{-11}	6.0×10^{-7}	5.0×10^{-5}
AR-coated QE in %	90	98	81
λ_p in µm	4.64	8.26	14.0
D* in cm Hz$^{1/2}$/W	3.0×10^{11}	9.3×10^{10}	5.0×10^{10}

Key Words: CrIS, Sounder, Large HgCdTe Detectors

1.0 INTRODUCTION

This document outlines the data collected during the EDU2 Module testing of all three FPMAs (SWIR, MWIR & LWIR). Each module is tested separately in the same dedicated CrIS nitrogen heli-tran Dewar. Test cables were made to integrate with the flight hardware that was available during test. Tests that were highly dependent on the flight-cable design such as cross-talk and phase delay were omitted and will be captured during the EDU3 phase. The Circuit Card Assembly (CCA) contains the warm amplifier and the second stage 300Hz High Pass filter. The CCA also provides the biases for the cold JFET pair on the cold electronics Ceramic Multilayer Board (CMLB). During some tests, the second stage coupling capacitor was defeated in order to collect DC data in the absence of the 30+kHz chopper being designed for EDU3.

2.0 CrIS DETECTOR PREAMPLIFIER MODULE

The Flight configuration for the CrIS Detector Preamplifier Module (DPM) consists of three spectrally separate (SWIR, MWIR and LWIR) FPMAs, three (SWIR, MWIR and LWIR) signal flex cable assemblies, a warm signal flex cable /vacuum bulk head assembly, and the DPM warm electronics circuit card assemblies (CCAs) as shown in figure 1. Each FPMA contains the array of nine 1000 μm diameter PV detectors with their associated cold electronics, a detector optics assembly, and two flex cable assemblies with interface connectors. The FPA modules (detector arrays, detector optics assemblies, JFET buffer and feedback resistor portions of the transimpedance preamplifier, and flex cable assemblies) are cooled to cryogenic temperatures by the detector cooler module. The cryogenic portions of the DPM (FPA Modules, and Signal Flex Cable Assemblies) mate to the ambient temperature portions of the DPM (warm signal flex cable assembly and the ambient temperature portions of the transimpedance amplifier, mounted within the CCAs) through the vacuum bulk head assembly mounted on the detector cooler module housing.

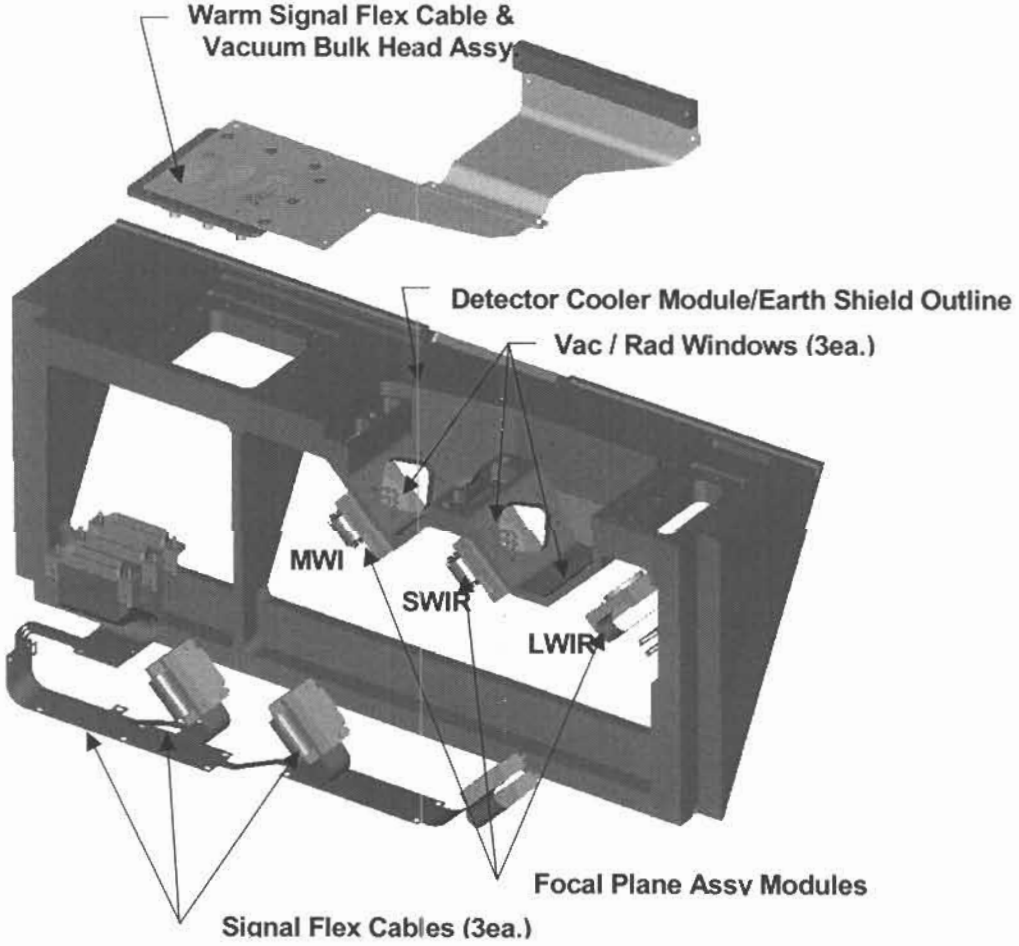

Figure 1 CrIS Detector Preamplifier Module (Warm Electronics CCAs not shown)

3.0 EDU2 Module Detectors

3.1 Predicted Performance Based on Diode Screening Parameters

The nine best performing detectors per module, 27 in all, were chosen and integrated into the FPMAz. Tables 3-5 lists the identification of the detectors and their predicted performance based on detector screening data.

Table 3 LWIR Detector Parameters

LWIR Parameters				Aimp = 8.89e-4 cm^2		
Channel	Wafer & ID	QE 9um	RoA_{opt} ($ohmcm^2$)	Id in A	λ_c in µm	i_n (6kHz)
1	3-284_8_8	68.7%	1.34E+00	6.81E-05	14.9	5.51E-12
2	3-288_10_5	71.2%	1.14E+00	5.99E-05	15.2	4.91E-12
3	3-284_8_1	61.5%	1.37E+00	8.29E-05	15.2	8.79E-12
4	3-284_11_5	70.0%	1.40E+00	5.02E-05	15.0	N/A
5	3-284_3_6	67.8%	1.44E+00	7.12E-05	N/A	7.16E-12
6	3-284_3_1	66.2%	1.25E+00	9.46E-05	15.1	7.10E-12
7	3-284_5_1	64.5%	1.20E+00	9.38E-05	N/A	9.20E-12
8	3-284_11_8	61.5%	1.51E+00	4.68E-05	14.9	N/A
9	3-284_4_6	68.7%	1.39E+00	7.36E-05	14.9	5.59E-12

Table 4 MWIR Detector Parameters

MWIR Parameters				Aimp = 8.89e-4 cm^2		
Channel	Wafer & ID	QE 8um	RoA_{opt} (ohm-cm^2)	Id in A	λ_c in µm	i_n (12kHz)
1	2-1241-7_5	71.5%	1.12E+02	6.96E-07	9.10	1.48E-12
2	2-1241-6_3	72.1%	1.18E+02	7.14E-07	9.08	1.49E-12
3	2-1241-5_10	70.8%	1.45E+02	5.07E-07	9.01	7.77E-13
4	2-1241-11_6	71.9%	1.31E+02	4.89E-07	9.08	1.08E-12
5	2-1241-8_4	70.3%	1.22E+02	6.24E-07	9.10	1.16E-12
6	2-1241-12_2	69.5%	1.84E+02	3.58E-07	8.97	9.03E-13
7	2-1241-4_3	69.7%	1.28E+02	6.57E-07	9.06	1.41E-12
8	2-1241-5_3	71.4%	1.35E+02	6.20E-07	9.07	1.44E-12
9	2-1241-8_6	71.2%	1.26E+02	5.40E-07	9.11	1.19E-12

Table 5 SWIR Detector Parameters

SWIR Parameters				Aimp = 8.89e-4 cm^2		
Channel	Wafer & ID	QE 3.5um	RoA_{opt} (ohm-cm^2)	Id in A	λ_c in µm	i_n (20kHz)
1	1219-6_10	80.4%	9.71E+06	1.14E-11	5.33	
2	1219-7_6	83.8%	1.21E+07	2.11E-11	5.06	
3	1219-8_3	81.4%	1.80E+07	8.10E-12	5.10	
4	1219-9_7	83.8%	2.53E+07	6.85E-12	5.04	
5	1219-8_5	79.5%	6.53E+06	1.56E-11	5.38	
6	1219-11_3	80.9%	8.26E+06	1.33E-11	5.38	
7	1219-10_8	80.6%	7.87E+06	2.35E-11	5.38	
8	1219-12_6	77.8%	6.02E+06	1.58E-11	5.34	
9	1219-7_2	80.3%	4.96E+06	2.51E-11	5.09	

Due to the low yield on the LWIR detector, the EDU3 phase will develop a LWIR with a smaller implant area and improved signal to noise.

4.0 Experimental Setup

A total of three experimental setups were required to test all five parameters in Table A. The nonlinearity, dynamic range and a portion of the data required for the D* calculation require equipment detailed in Setup A. The noise spectral density and the noise required for the D* calculation require the equipment in Setup B and the power measurements require Setup C.

4.1 Setup A (DC Configuration)

Figure 2 illustrates the setup required to Test the Nonlinearity and the Dynamic Range of the entire FPMA including all amplifier stages. The CCA has nine BNC receptacles – one for each of the nine channels. For this setup, the A/C coupling capacitor on the second stage is defeated by soldering a short over the capacitor's leads. By defeating the coupling capacitor, a DC output is achieved and is monitored on a voltmeter.

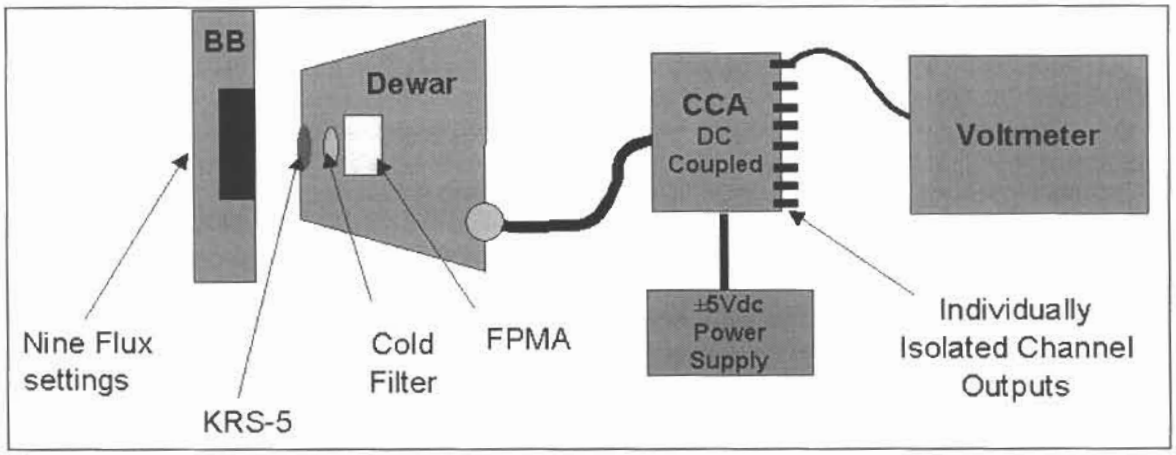

Figure 2 Test Setup A

4.2 Setup B (AC Configuration)

An A/C configuration is required for the spectral noise test and for data required for the D* calculation. The coupling capacitor is not defeated for this measurement. One by one, the nine CCA output channels are connected to an HP3562A Dynamic Signal Analyzer. The data is then transferred electronically to a PC and stored.

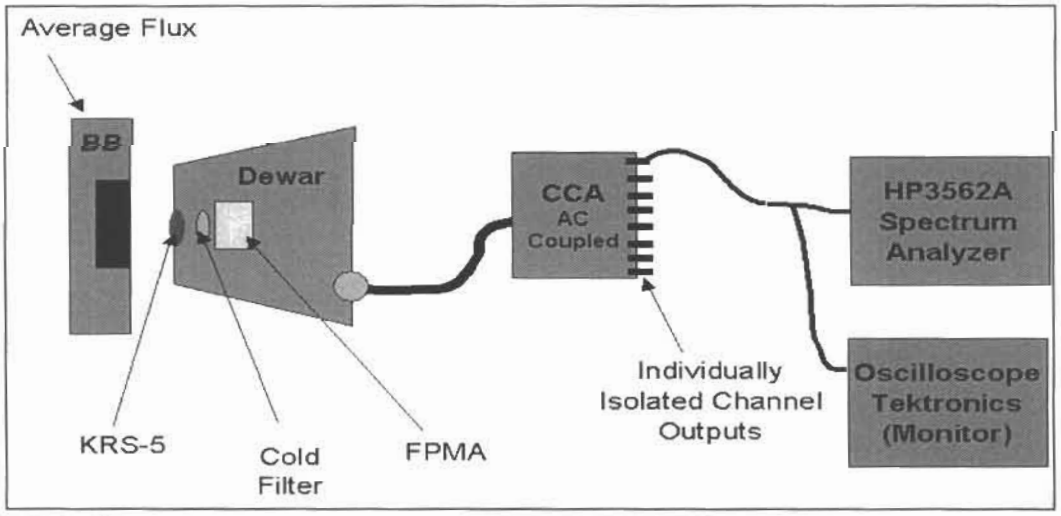

Figure 3 Test Setup B

4.3 Setup C (Power Configuration)

The Ambient Power Dissipation tests require a current meter in series with the +/- 5volt supply.

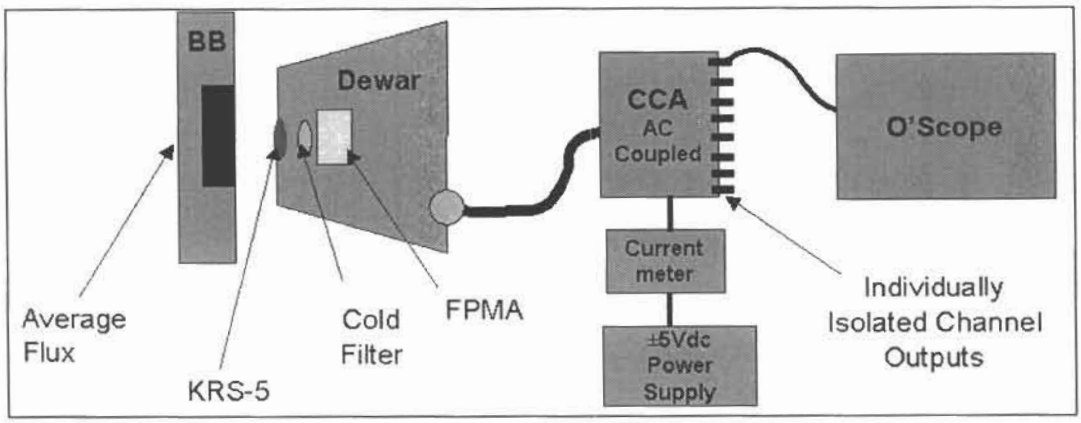

Figure 4 Test Setup C Power Dissipation

5.0 LWIR FPMA Data

The LWIR FPMA was cooled to 81K, biased at –60mV. For the non linearity test, the diodes were illuminated with nine flux values between 2.8E17 photons/cm^2*s and 4.0E17 photons/cm^2*s. For the D* calculation and noise measurements in the nominal operating flux of 3.5 E17 photons/cm^2*s was used. These flux values were achieved using an Electro-Optical Industries (EOI) Black Body mounted external to the Dewar. The Dewar flux is calibrated using diode with a known quantum efficiency at 81K.

Figure 5 illustrates the linearity of the FPMA. Each diode is illuminated and the CCA output voltage is recorded for nine different flux values. The outputs are then plotted as a function of flux. Figure 5 illustrates the deviations from the linear least square fit of the original data as a function of flux. The mean and standard deviation of the nonlinearity for the operating channels (excluding channel 1) was 0.16 +/-0.11%.

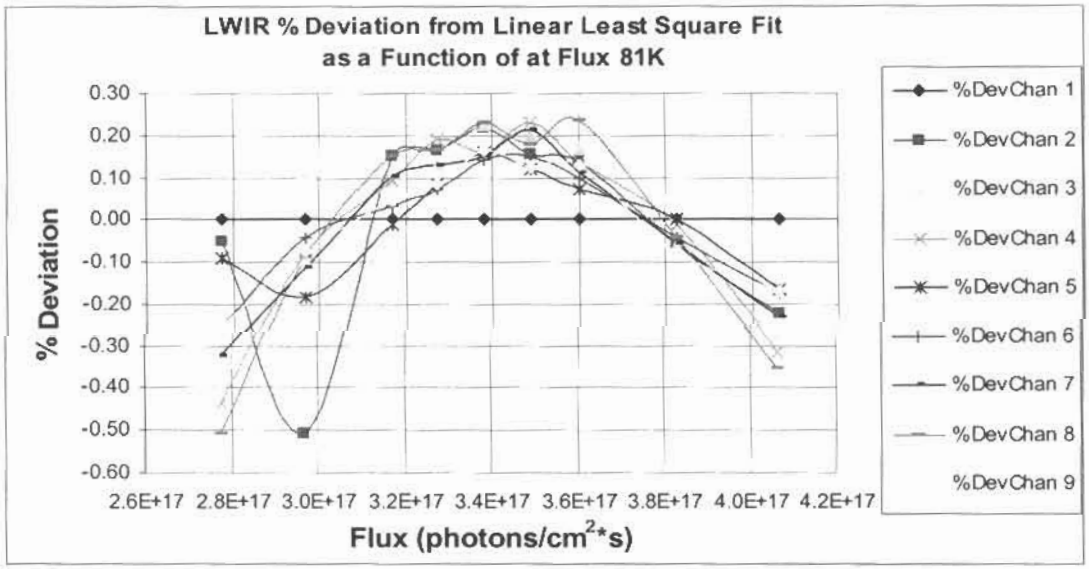

Figure 5

The noise spectral density for all nine channels is plotted in Figure 6. For LWIR, the electrical band of interest is 6.5-10.95kHz. The CCA is AC coupled for this measurement, which explains the 300Hz roll on of the high pass filter.

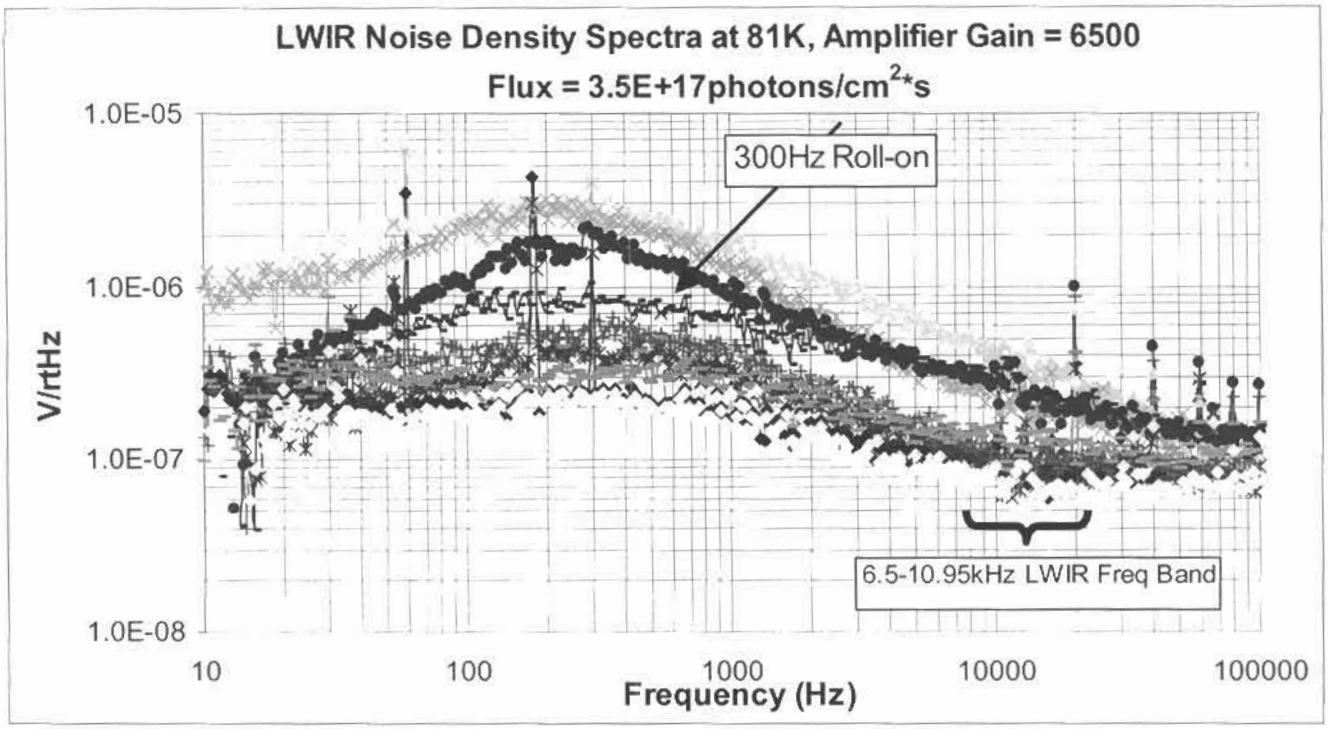

Figure 6 LWIR Noise Density

To calculate D* at the peak wavelength of 14.01μm, the integrated noise within the band of interest is used. The CCA voltage response at average flux and a relative photon response profile are used to generate a spectral response curve. With this data and the integrated noise under the band, a channel's D* can be calculated as per equation 1.

$$D^*(\lambda_p, f) = \frac{\Re * \sqrt{A_{\text{det}}} * \sqrt{\Delta f}}{V_n} (Jones)$$

Equation 1.

The D* performance of the EDU2 FPMA diodes are listed in Table 6. For completeness, the maximum D* and the wavelength where this performance was achieved is listed in the table as well.

Table 6

Channel	D* (14.01μm)	Max D*	@ Wavelength (μm)
Channel 1	N/F	N/F	-------
Channel 2	7.18E+09	9.26E+09	13.3
Channel 3	1.55E+10	1.68E+10	13.6
Channel 4	3.25E+10	3.72E+10	13.2
Channel 5	1.62E+10	1.80E+10	13.0
Channel 6	3.45E+10	3.84E+10	13.0
Channel 7	1.20E+10	1.34E+10	13.1
Channel 8	2.31E+10	2.71E+10	13.0
Channel 9	4.87E+10	5.41E+10	13.3

The spectral D* as a function of wavelength is plotted in Figure 7. The average D* at 14.01μm was 2.4E10 +/-1.4E10 Jones.

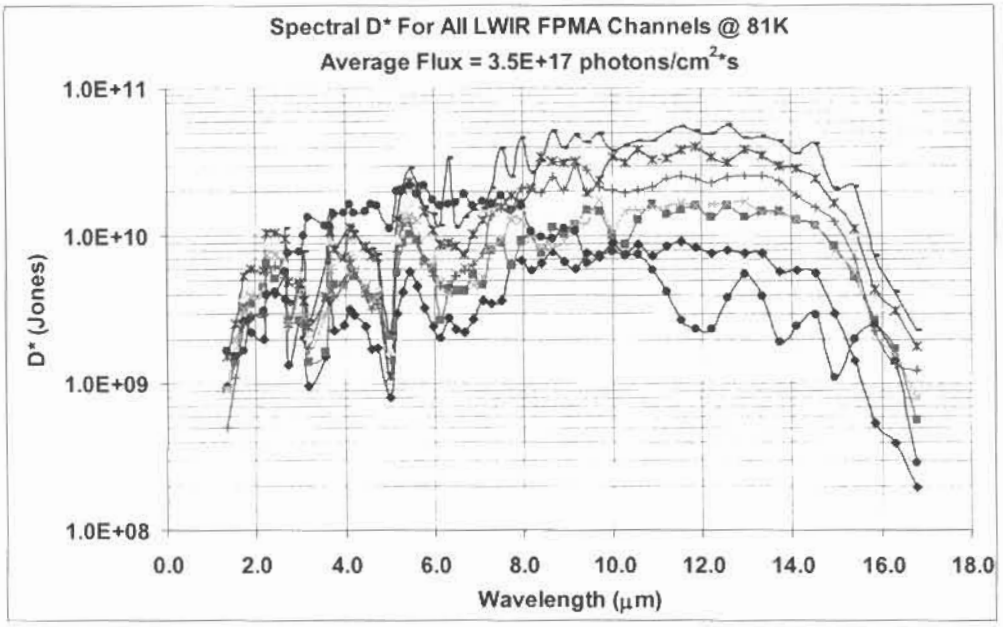

Figure 7 LWIR Spectral D* at 81K and average flux

The LWIR power dissipation measurement required Test Setup C. The current on the 5V DC CCA power supply is measured and multiplied by the 5V supply value to yield the module's total power dissipation. The measured power dissipation was 0.395W. The cooler's power consumption flow down requirement a total of 3.3W for all three modules combined.

6.0 MWIR FPMA Data

The MWIR FPMA was cooled to 98K, biased at –60mV. For the nonlinearity test, the diodes were illuminated with nine flux values between 5.11E16 photons/cm^2*s and 7.36E17 photons/cm^2*s. For the D* calculation and noise measurements in the nominal operating flux of 6.21E17 photons/cm^2*s was used. These flux values were achieved using an Electro-Optical Industries (EOI) Black Body mounted external to the Dewar. The Dewar flux is calibrated using a diode with known quantum efficiency at 98K.

Figure 8 illustrates the linearity of the MWIR FPMA. Each diode is illuminated and the CCA output voltage is recorded for nine different flux values. The outputs are then plotted as a function of flux. Figure 8 shows the deviations from the linear least square fit of the original data as a function of flux. The mean and standard deviation of the nonlinearity the nine channels was 0.04 +/-0.03%.

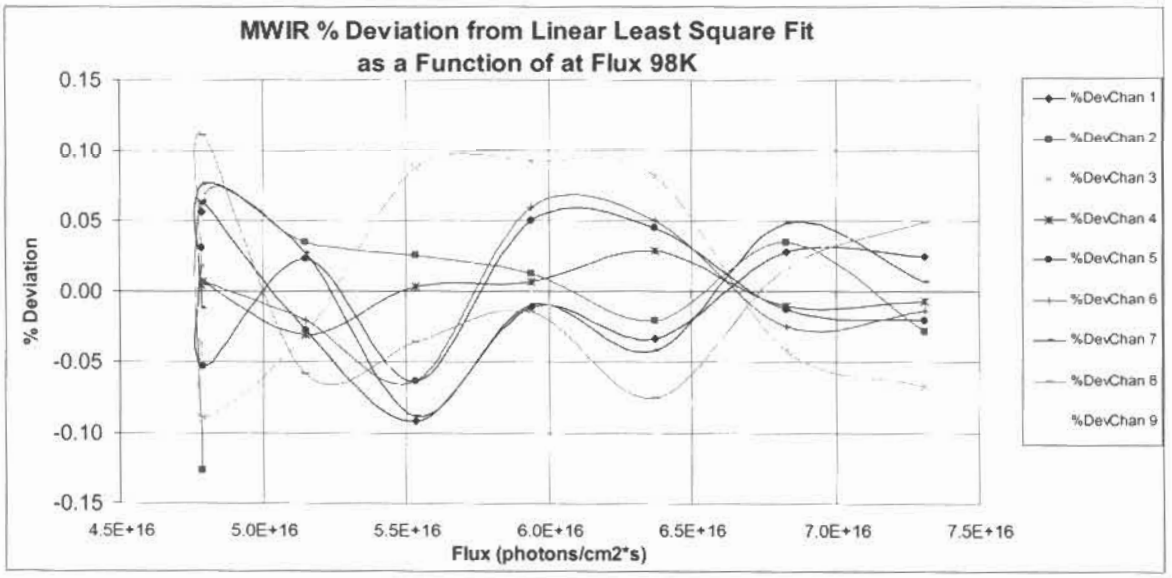

Figure 8 MWIR Nonlinearity

The noise spectral density for all nine channels is plotted in Figure 9. For MWIR, the electrical band of interest is 12.10-17.5kHz. The CCA is A/C coupled for this measurement, which explains the 300Hz roll on of the high pass filter.

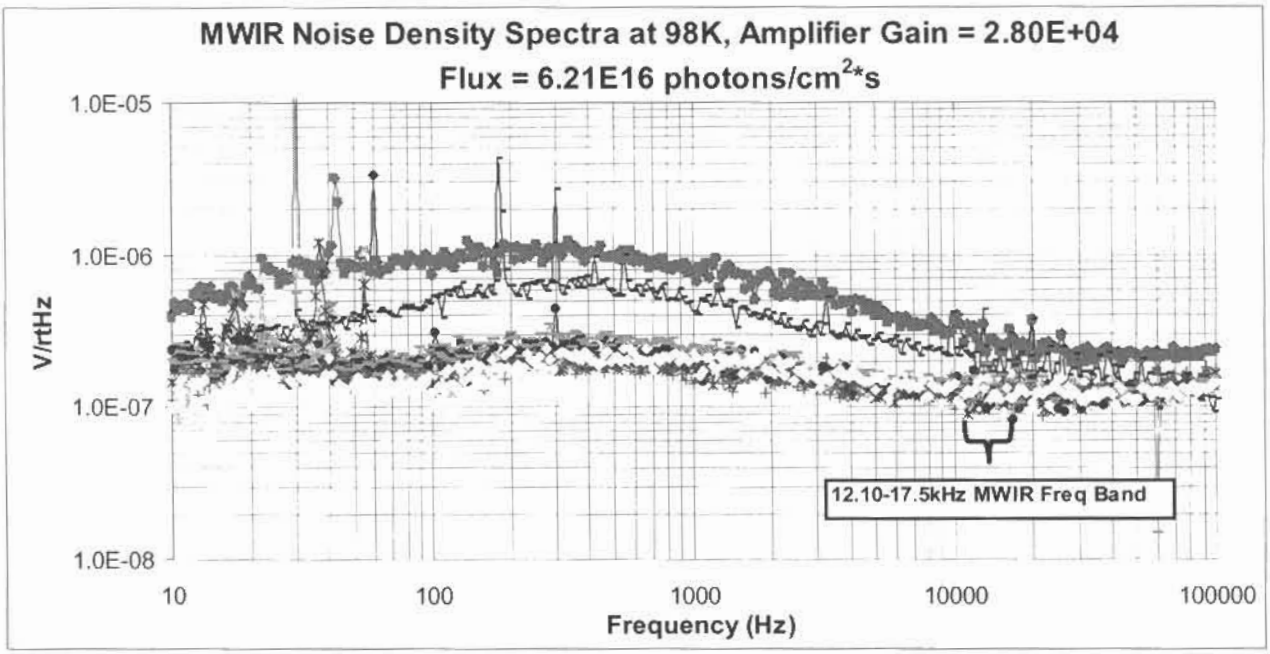

Figure 9 MWIR Noise Spectral Density at 98K and Average Flux

To calculate D* at the peak wavelength of 8.26μm, the integrated noise within the band of interest is used. The CCA voltage response at average flux and a relative photon response profile are used to generate a spectral response curve. With this data and the integrated noise under the band, a channel's D* can be calculated as per equation 1. The LWIR D* performance at 8.26 μm is listed in Table 7.

Table 7

Channel	D*(8.26μm)	Max D*	@ Wavelength (μm)
Channel 1	4.1E+10	4.3E+10	8.02
Channel 2	8.1E+10	8.7E+10	7.99
Channel 3	9.4E+10	1.1E+11	7.91
Channel 4	9.1E+10	1.1E+10	7.95
Channel 5	9.6E+10	1.02E+11	7.99
Channel 6	8.7E+10	9.92E+10	7.84
Channel 7	4.8E+10	5.26E+10	7.95
Channel 8	7.3E+10	7.86E+10	8.10
Channel 9	8.6E+10	9.19E+10	7.99

The spectral D* as a function of wavelength is plotted in Figure 10. The average D* at 8.26μm was 7.7E10 +/- 2.0E10 Jones.

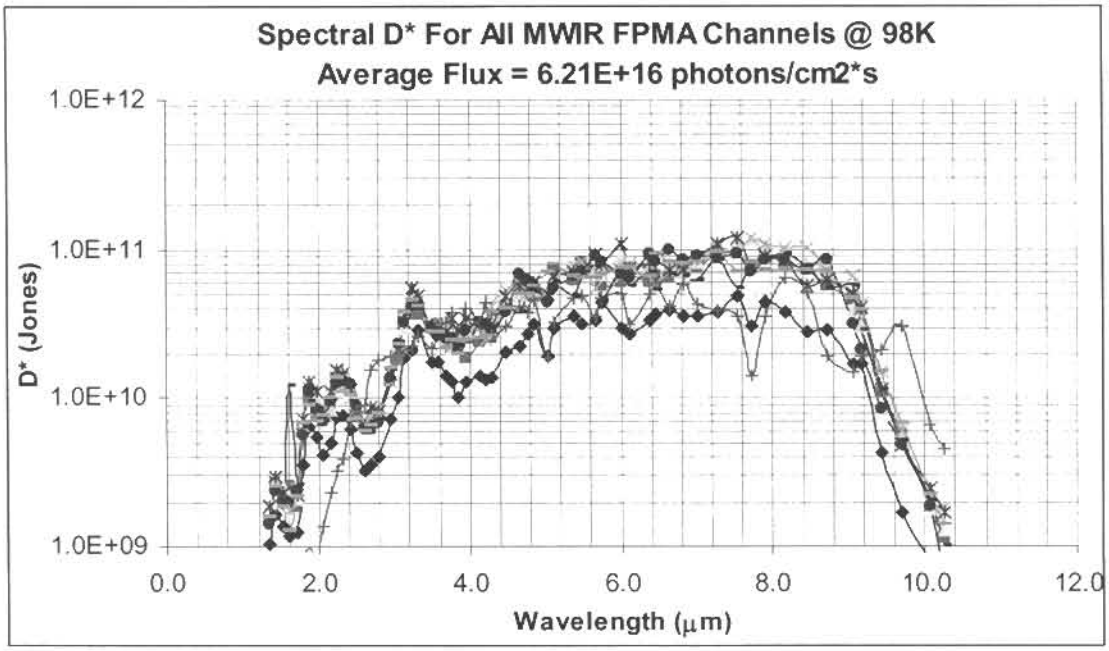

Figure 10 MWIR Spectral D*

6.0 SWIR FPMA Data

The SWIR FPMA was cooled to 98K, biased at –5.0mV. For the nonlinearity test, the diodes were illuminated with nine flux values between 1.49E+15 photons/cm^2*s and 2.12E+15 photons/cm^2*s. For the D* calculation and noise measurements in the nominal operating flux of 1.80E+15 photons/cm^2*s was used. These flux values were achieved using an Electro-Optical Industries (EOI) Black Body mounted external to the Dewar. The Dewar flux is calibrated using a diode with known quantum efficiency at 98K

Figure 11 illustrates the linearity of the FPMA. Each diode is illuminated and the CCA output voltage is recorded for nine different flux values. The outputs are then plotted as a function of flux. Figure 11 illustrates the deviations from the linear least square fit of the original data as a function of flux. The mean and standard deviation of the nonlinearity for the operating channels (excluding channel 1) was 0.07 +/-0.04%.

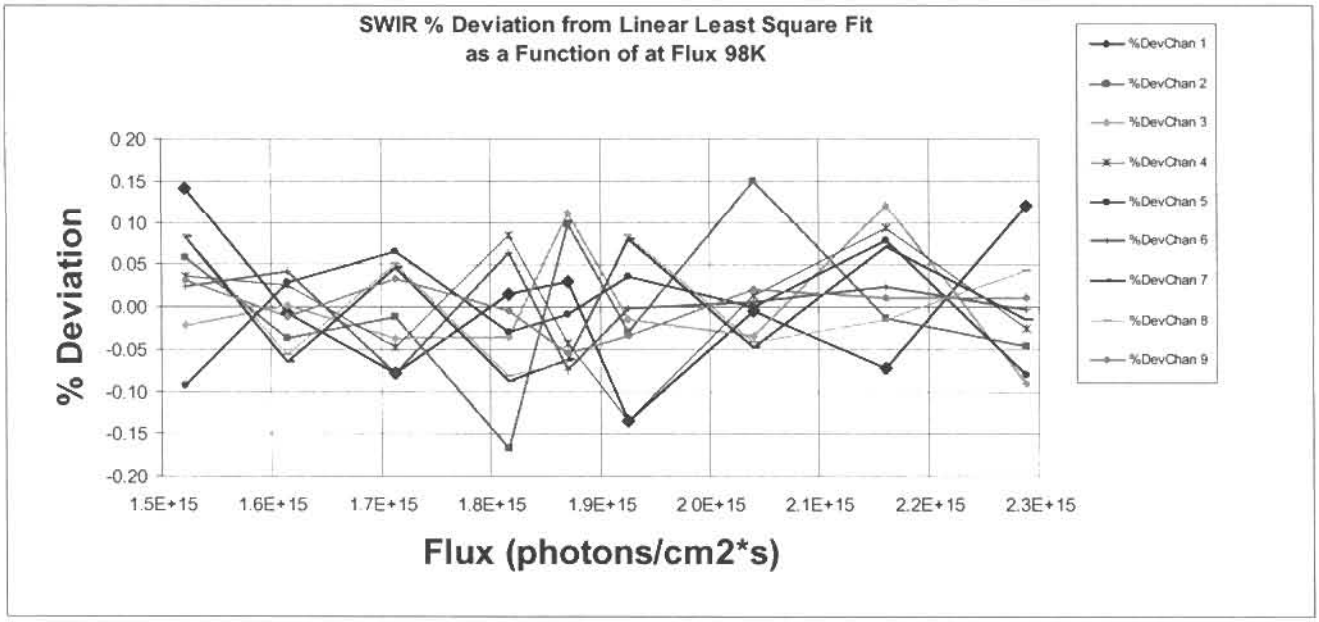

Figure 11 SWIR Nonlinearity

The noise spectral density for all nine channels is plotted in Figure 12. For SWIR, the electrical band of interest is 21.55-25.5kHz. The CCA is A/C coupled for this measurement, which explains the 300Hz roll on of the high pass filter.

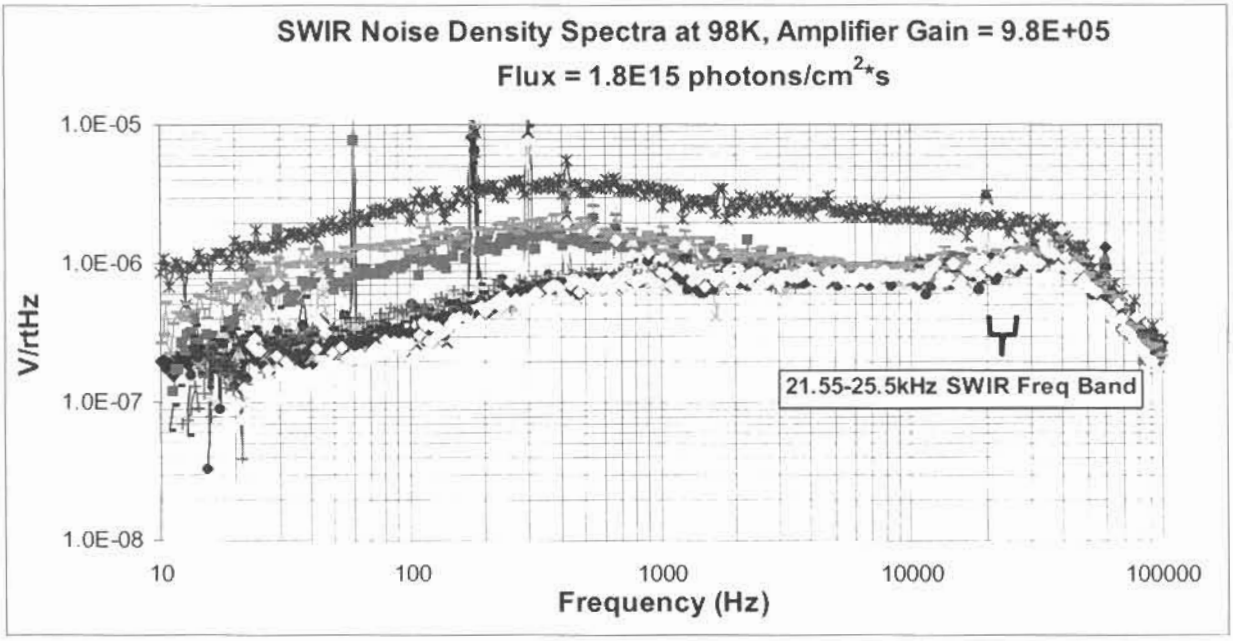

Figure 12 SWIR Noise Spectral Density

To calculate D* at the peak wavelength of 4.64μm, the integrated noise within the band of interest is used. The CCA voltage response at average flux and a relative photon response profile are used to generate a spectral response curve. With this data and the integrated noise under the band, a channel's D* can be calculated as per equation 1. The MWIR D* performance at 4.65μm is listed in Table 8.

Table 8

Channel	D* (4.64μm)	Max D*	@ Wavelength (μm)
Channel 1	2.73E+11	2.78E+11	4.73
Channel 2	2.75E+11	2.83E+11	4.52
Channel 3	3.10E+11	3.16E+11	4.77
Channel 4	1.43E+11	1.47E+11	4.52
Channel 5	3.10E+11	3.16E+11	4.81
Channel 6	3.20E+11	3.23E+11	4.70
Channel 7	3.09E+11	3.14E+11	4.75
Channel 8	2.61E+11	2.66E+11	4.74
Channel 9	2.99E+11	3.07E+11	4.74

The spectral D* as a function of wavelength is plotted in Figure 13. The average D* at 4.64μm was 2.8E11 +/- 5.4E10 Jones.

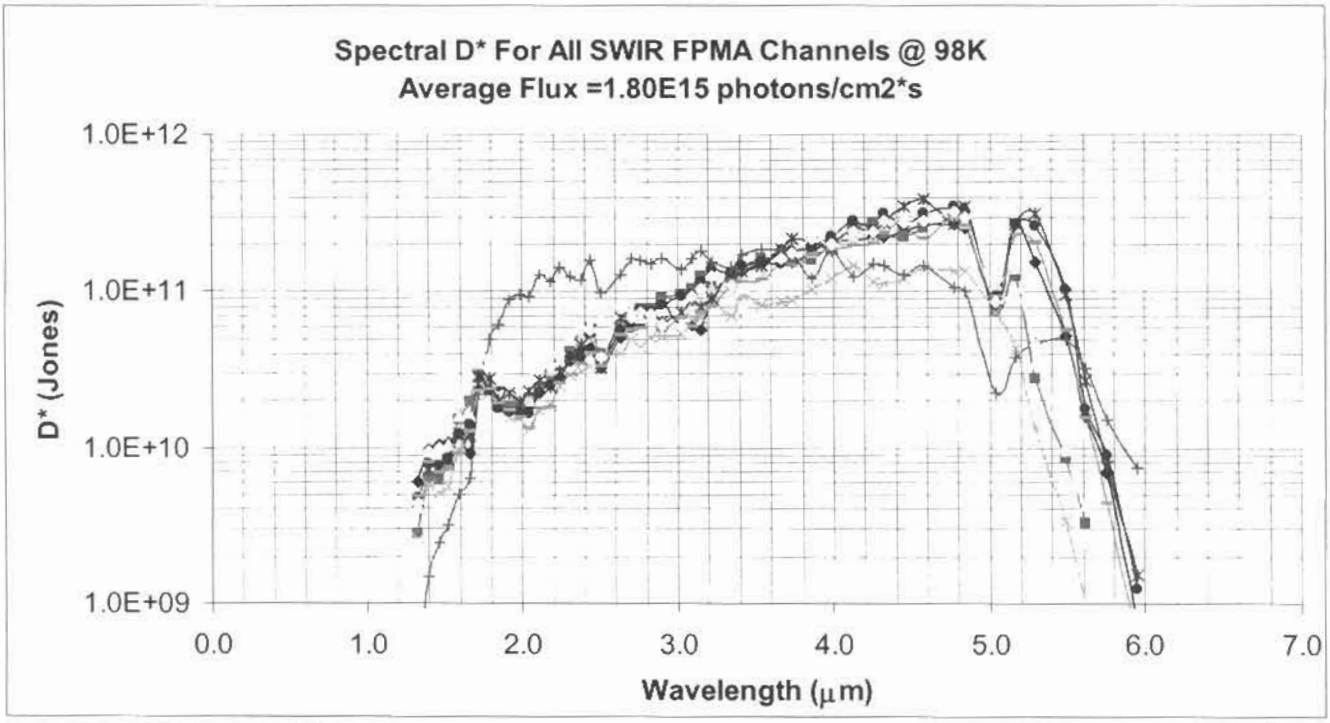

Figure 13 SWIR Spectral D*

7.0 Dynamic Range

The cold and warm electronics were designed such that the CCA Channel outputs would have a nominal range of 0.5V peak-to-peak between minimum and maximum flux. The Dynamic Range of all three modules is listed in Table 8

Table 9

FPMA Dynamic Range	
LWIR	0.731+/- 0.07V
MWIR	0.676 +/- 0.02V
SWIR	0.780 +/- 0.04V

8.0 DPM Ambient Power Dissipation

The power dissipation measurement required Test Setup C. The current on the 5V DC CCA power supply is measured and multiplied by the 5V supply value to yield the module's total power dissipation. The measured power for all three modules is listed in table 9. The cooler's power consumption flow down requirement is a total of 3.3W for all three modules combined. The total power disspation for a all three modules is 1.176 W.

Table 10

Ambient Power Disspation	
LWIR	0.395W
MWIR	0.390W
SWIR	0.391W

9.0 SUMMARY

The testing of the CrIS EDU2 FPMAs yielded data that was typical of the detectors as stand alone devices. The $Hg_{1-x}Cd_xTe$ detectors chosen for the CrIS EDU2 FPMAs have been successfully integrated into a fully functional module platform while accommodating our customer's mechanical and electrical flow-down requirements. Detector-screening parameters developed during the EDU1 phase have been utilized during the EDU2 FPMA build. Data collected during the EDU2 phase validates the diode screening and selection process that will be implemented for EDU3. The data shows the benefits of utilizing PV technology for space-based applications. FPMA linearity performance is 0.16 +/-0.11% for LWIR, 0.04 +/-0.03% for MWIR and 0.07 +/-0.04% for SWIR. FPMA D* performance is 2.4E+10 +/- 1.4E+10 Jones at 14.01μm for LWIR, 7.7E+10 +/-2.0E+10 Jones at 8.26μm for MWIR, and 2.8E+11 +/-5.4E+10 Jones at 4.64μm for SWIR. Changes to detector architecture for LWIR will enhance operability and improve detector yields in the future.

10.0 REFERENCES

1. J.M. Arias, J.G. Pasko, M. Zandian, L.J. Kozlowski and R.E. DeWames, *Optical Engineering* **33**, 1422(1994).
2. J.M. Arias, J.G. Pasko, M. Zandian, J. Bajaj, L.J. Kozlowski, R.E. DeWames, and W.E. Tennant, "Proceedings of SPIE Symposia on Producibility of II-VI Materials and Devices", Vol. 2228, p. 210 (1994).
3. J. Bajaj, J.M. Arias, M. Zandian, J.G. Pasko, L.J. Kozlowski, R.E. DeWames, W.E. Tennant, *J. Electron. Mater.* **24**, 1067 (1995).
4. J. Bajaj, J.M. Arias, M. Zandian, J.G. Pasko, L.J. Kozlowski, R.E. DeWames and W.E. Tennant, *J. Electron. Mater.* **25**, 1394 (1996).
5. D.D. Edwall, M. Zandian, A.C. Chen, and J. M. Arias, *J. Electron. Mater.* **26**, 493 (1997).
6. A.I. D'Souza, L.C. Dawson, E.J. Anderson, A.D. Markum, W.E. Tennant, L.O. Bubulac, M. Zandian, J.G. Pasko, W.V. McLevige, D.D. Edwall, *J. Electron. Mater.* 26, 656 (1997).

Cross-Track Infrared Sounder FPMA Performance

S. Masterjohn , A.I. D'Souza, L.C. Dawson, P. Dolan
Boeing Sensor Products, 3370 Miraloma Avenue, Anaheim, CA 92803

P.S. Wijewarnasuriya
Rockwell Scientific Company, 1049 Camino Dos Rios, Thousand Oaks, CA 91360

J. Ehlert
ITT Aerospace/Communications Division, Ft. Wayne, IN

ABSTRACT

The Cross-track Infrared Sounder (CrIS) is one of many instruments that comprise the National Polar-orbiting Operational Environmental Satellite System (NPOESS). The CrIS instrument consists of a Michelson interferometer infrared sounder that is sensitive to wavelengths between 3.5 and 16 microns. This spectral band is achieved by using three separate Focal Plane Module Assemblies (FPMAs) referred to as the Short Wave Infrared module (SWIR, $\lambda_c \sim 5$ µm at 98K), the Mid Wave Infrared module (MWIR, $\lambda_c \sim 9$ µm at 98K), and the Long Wave Infrared module (LWIR, $\lambda_c \sim 16$ µm at 81K). The CrIS instrument measures the earth radiances at high spectral resolution, using the data to provide pressure, temperature and moisture profiles of the atmosphere. The CrIS instrument will help improve both global and regional predictions of weather patterns, storm tracks, and precipitation. The CrIS program selected the use of photovoltaic (PV) detectors for all three spectral bands. PV technology outperforms photoconductive detectors in terms of high sensitivity and linearity. Each FPMA consists of a 3x3 detector-matrix of 9 fields of view (FOV). Each detector is 1,000um in diameter and has its own cold preamplifier, warm post amplifier and high pass filter. This paper describes the performance for all three modules that together form the CrIS Engineering Development Unit 2 (EDU2) Detector Preamp Assembly (DPM).

Molecular Beam Epitaxy (MBE) is used to grow the appropriate bandgap n-type $Hg_{1-x}Cd_xTe$ on lattice matched CdZnTe. SWIR, MWIR and LWIR 1000 µm diameter detectors have been manufactured using the Lateral Collection Diode (LCD) architecture[1-5]. Custom pre-amplifiers have been designed to interface with the large SWIR, MWIR and LWIR detectors. The operating temperature is above 78K, permitting the use of passive radiators in spacecraft to cool the detectors. Recently, all three FPMAs were completed and tested. The tests performed on each module are listed in Table 1.

Table 1

FPMA Testing
1. Response Nonlinearity
2. Noise Spectral Density
3. D* Calculation
4. Ambient Power Dissipation
5. Dynamic Range

Prior to building the FPMAs, the candidate detectors were screened for properties consistent with those listed in Table 2[6]. The D* values in Table B are calculated at the CrIS program peak wavelength specified for each spectral band.

Table 2

	SWIR	MWIR	LWIR
Operating Temperature (K)	98	98	81
λ_c in µm	5.02	9.89	15.9
R_oA_{opt} in ohm-cm^2	9.0×10^{6}	1.0×10^{2}	1.5×10^{0}
I_d at V_d = -0.1 V	1.0×10^{-11}	6.0×10^{-7}	5.0×10^{-5}
AR-coated QE in %	90	98	81
λ_p in µm	4.64	8.26	14.0
D* in cm Hz$^{1/2}$/W	3.0×10^{11}	9.3×10^{10}	5.0×10^{10}

Key Words: CrIS, Sounder, Large HgCdTe Detectors

1.0 INTRODUCTION

This document outlines the data collected during the EDU2 Module testing of all three FPMAs (SWIR, MWIR & LWIR). Each module is tested separately in the same dedicated CrIS nitrogen heli-tran Dewar. Test cables were made to integrate with the flight hardware that was available during test. Tests that were highly dependent on the flight-cable design such as cross-talk and phase delay were omitted and will be captured during the EDU3 phase. The Circuit Card Assembly (CCA) contains the warm amplifier and the second stage 300Hz High Pass filter. The CCA also provides the biases for the cold JFET pair on the cold electronics Ceramic Multilayer Board (CMLB). During some tests, the second stage coupling capacitor was defeated in order to collect DC data in the absence of the 30+kHz chopper being designed for EDU3.

2.0 CrIS DETECTOR PREAMPLIFIER MODULE

The Flight configuration for the CrIS Detector Preamplifier Module (DPM) consists of three spectrally separate (SWIR, MWIR and LWIR) FPMAs, three (SWIR, MWIR and LWIR) signal flex cable assemblies, a warm signal flex cable /vacuum bulk head assembly, and the DPM warm electronics circuit card assemblies (CCAs) as shown in figure 1. Each FPMA contains the array of nine 1000 μm diameter PV detectors with their associated cold electronics, a detector optics assembly, and two flex cable assemblies with interface connectors. The FPA modules (detector arrays, detector optics assemblies, JFET buffer and feedback resistor portions of the transimpedance preamplifier, and flex cable assemblies) are cooled to cryogenic temperatures by the detector cooler module. The cryogenic portions of the DPM (FPA Modules, and Signal Flex Cable Assemblies) mate to the ambient temperature portions of the DPM (warm signal flex cable assembly and the ambient temperature portions of the transimpedance amplifier, mounted within the CCAs) through the vacuum bulk head assembly mounted on the detector cooler module housing.

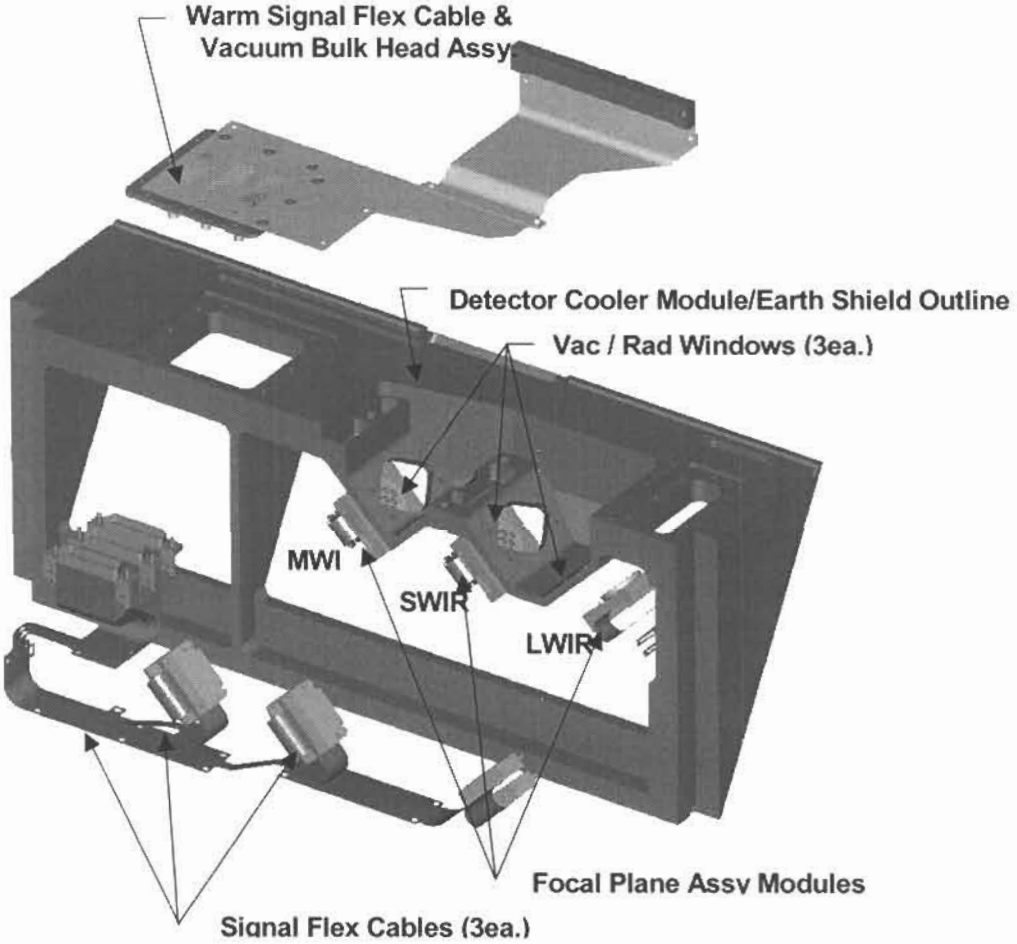

Figure 1 CrIS Detector Preamplifier Module (Warm Electronics CCAs not shown)

3.0 EDU2 Module Detectors

3.1 Predicted Performance Based on Diode Screening Parameters

The nine best performing detectors per module, 27 in all, were chosen and integrated into the FPMAz. Tables 3-5 lists the identification of the detectors and their predicted performance based on detector screening data.

Table 3 LWIR Detector Parameters

LWIR Parameters				Aimp = 8.89e-4 cm^2		
Channel	Wafer & ID	QE 9um	RoA_{opt} ($ohmcm^2$)	Id in A	λ_c in µm	i_n (6kHz)
1	3-284_8_8	68.7%	1.34E+00	6.81E-05	14.9	5.51E-12
2	3-288_10_5	71.2%	1.14E+00	5.99E-05	15.2	4.91E-12
3	3-284_8_1	61.5%	1.37E+00	8.29E-05	15.2	8.79E-12
4	3-284_11_5	70.0%	1.40E+00	5.02E-05	15.0	N/A
5	3-284_3_6	67.8%	1.44E+00	7.12E-05	N/A	7.16E-12
6	3-284_3_1	66.2%	1.25E+00	9.46E-05	15.1	7.10E-12
7	3-284_5_1	64.5%	1.20E+00	9.38E-05	N/A	9.20E-12
8	3-284_11_8	61.5%	1.51E+00	4.68E-05	14.9	N/A
9	3-284_4_6	68.7%	1.39E+00	7.36E-05	14.9	5.59E-12

Table 4 MWIR Detector Parameters

MWIR Parameters				Aimp = 8.89e-4 cm^2		
Channel	Wafer & ID	QE 8um	RoA_{opt} (ohm-cm^2)	Id in A	λ_c in µm	i_n (12kHz)
1	2-1241-7_5	71.5%	1.12E+02	6.96E-07	9.10	1.48E-12
2	2-1241-6_3	72.1%	1.18E+02	7.14E-07	9.08	1.49E-12
3	2-1241-5_10	70.8%	1.45E+02	5.07E-07	9.01	7.77E-13
4	2-1241-11_6	71.9%	1.31E+02	4.89E-07	9.08	1.08E-12
5	2-1241-8_4	70.3%	1.22E+02	6.24E-07	9.10	1.16E-12
6	2-1241-12_2	69.5%	1.84E+02	3.58E-07	8.97	9.03E-13
7	2-1241-4_3	69.7%	1.28E+02	6.57E-07	9.06	1.41E-12
8	2-1241-5_3	71.4%	1.35E+02	6.20E-07	9.07	1.44E-12
9	2-1241-8_6	71.2%	1.26E+02	5.40E-07	9.11	1.19E-12

Table 5 SWIR Detector Parameters

SWIR Parameters				Aimp = 8.89e-4 cm^2		
Channel	Wafer & ID	QE 3.5um	RoA_{opt} (ohm-cm^2)	Id in A	λ_c in µm	i_n (20kHz)
1	1219-6_10	80.4%	9.71E+06	1.14E-11	5.33	
2	1219-7_6	83.8%	1.21E+07	2.11E-11	5.06	
3	1219-8_3	81.4%	1.80E+07	8.10E-12	5.10	
4	1219-9_7	83.8%	2.53E+07	6.85E-12	5.04	
5	1219-8_5	79.5%	6.53E+06	1.56E-11	5.38	
6	1219-11_3	80.9%	8.26E+06	1.33E-11	5.38	
7	1219-10_8	80.6%	7.87E+06	2.35E-11	5.38	
8	1219-12_6	77.8%	6.02E+06	1.58E-11	5.34	
9	1219-7_2	80.3%	4.96E+06	2.51E-11	5.09	

Due to the low yield on the LWIR detector, the EDU3 phase will develop a LWIR with a smaller implant area and improved signal to noise.

4.0 Experimental Setup

A total of three experimental setups were required to test all five parameters in Table A. The nonlinearity, dynamic range and a portion of the data required for the D* calculation require equipment detailed in Setup A. The noise spectral density and the noise required for the D* calculation require the equipment in Setup B and the power measurements require Setup C.

4.1 Setup A (DC Configuration)

Figure 2 illustrates the setup required to Test the Nonlinearity and the Dynamic Range of the entire FPMA including all amplifier stages. The CCA has nine BNC receptacles – one for each of the nine channels. For this setup, the A/C coupling capacitor on the second stage is defeated by soldering a short over the capacitor's leads. By defeating the coupling capacitor, a DC output is achieved and is monitored on a voltmeter.

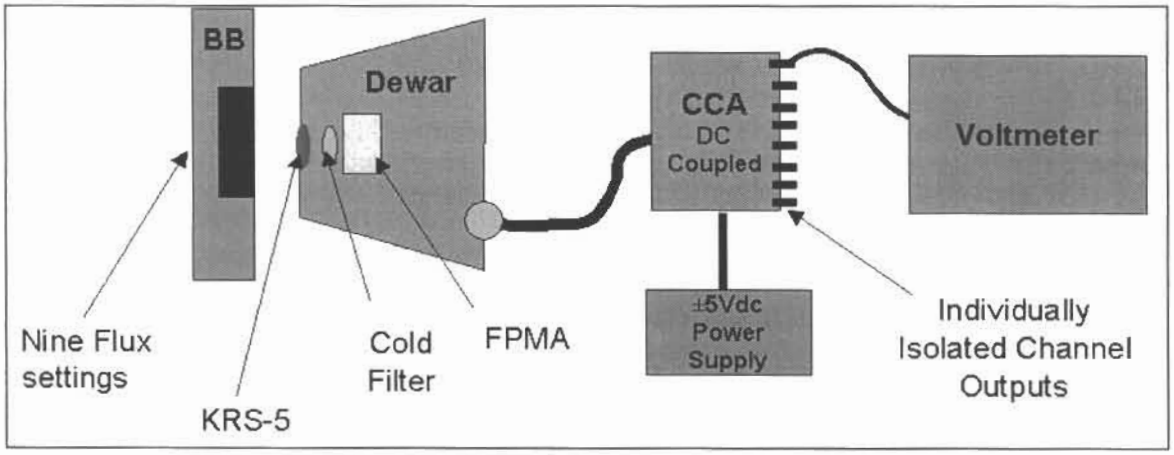

Figure 2 Test Setup A

4.2 Setup B (AC Configuration)

An A/C configuration is required for the spectral noise test and for data required for the D* calculation. The coupling capacitor is not defeated for this measurement. One by one, the nine CCA output channels are connected to an HP3562A Dynamic Signal Analyzer. The data is then transferred electronically to a PC and stored.

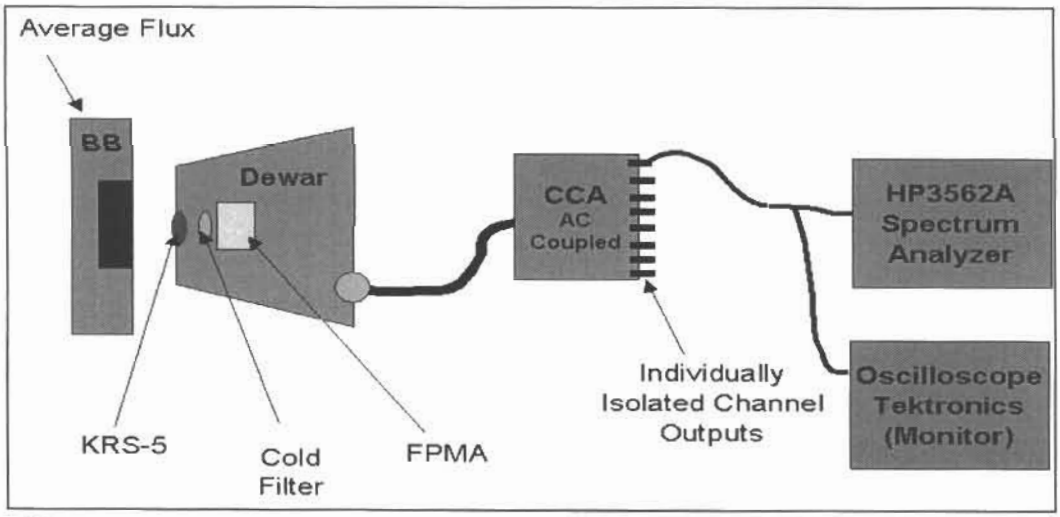

Figure 3 Test Setup B

4.3 Setup C (Power Configuration)

The Ambient Power Dissipation tests require a current meter in series with the +/- 5volt supply.

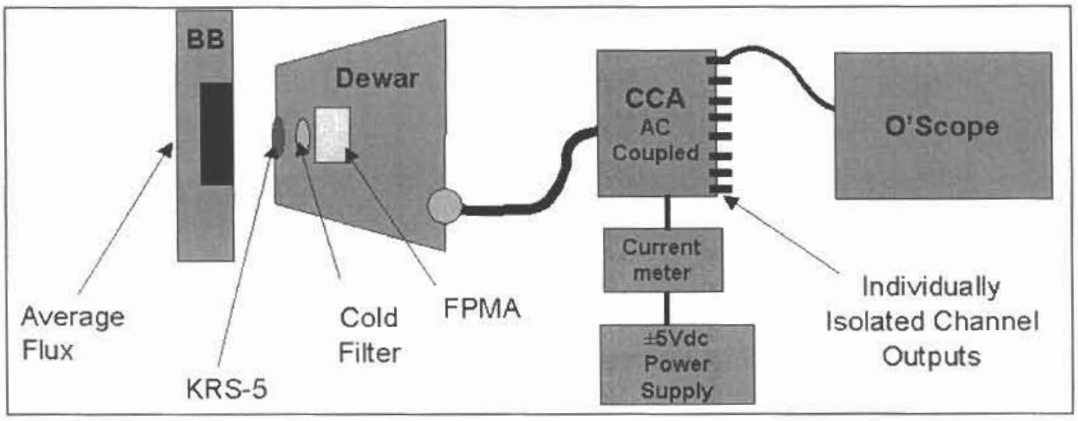

Figure 4 Test Setup C Power Dissipation

5.0 LWIR FPMA Data

The LWIR FPMA was cooled to 81K, biased at –60mV. For the non linearity test, the diodes were illuminated with nine flux values between 2.8E17 photons/cm^2*s and 4.0E17 photons/cm^2*s. For the D* calculation and noise measurements in the nominal operating flux of 3.5 E17 photons/cm^2*s was used. These flux values were achieved using an Electro-Optical Industries (EOI) Black Body mounted external to the Dewar. The Dewar flux is calibrated using diode with a known quantum efficiency at 81K.

Figure 5 illustrates the linearity of the FPMA. Each diode is illuminated and the CCA output voltage is recorded for nine different flux values. The outputs are then plotted as a function of flux. Figure 5 illustrates the deviations from the linear least square fit of the original data as a function of flux. The mean and standard deviation of the nonlinearity for the operating channels (excluding channel 1) was 0.16 +/-0.11%.

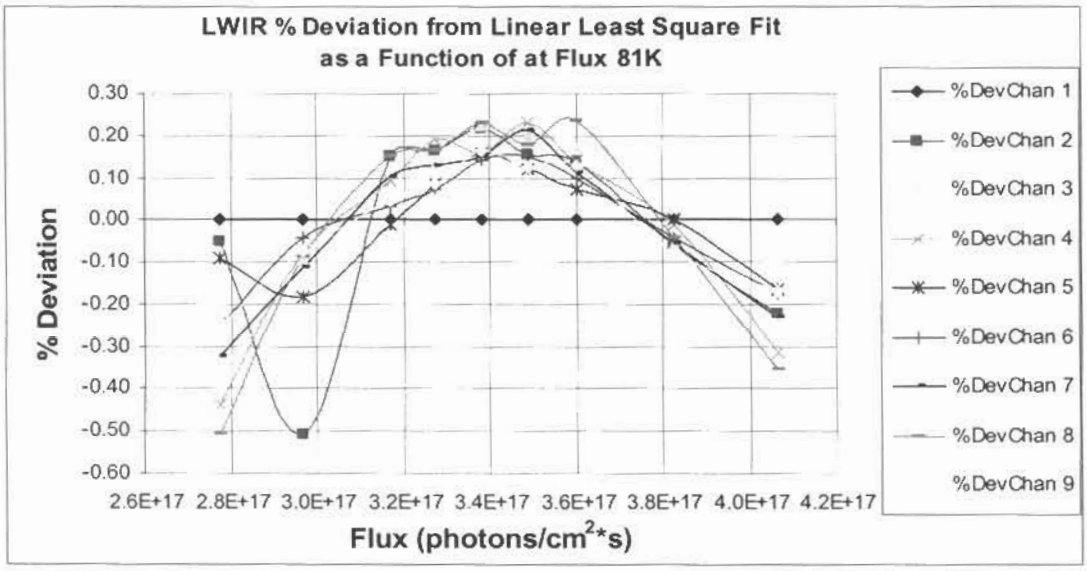

Figure 5

The noise spectral density for all nine channels is plotted in Figure 6. For LWIR, the electrical band of interest is 6.5-10.95kHz. The CCA is AC coupled for this measurement, which explains the 300Hz roll on of the high pass filter.

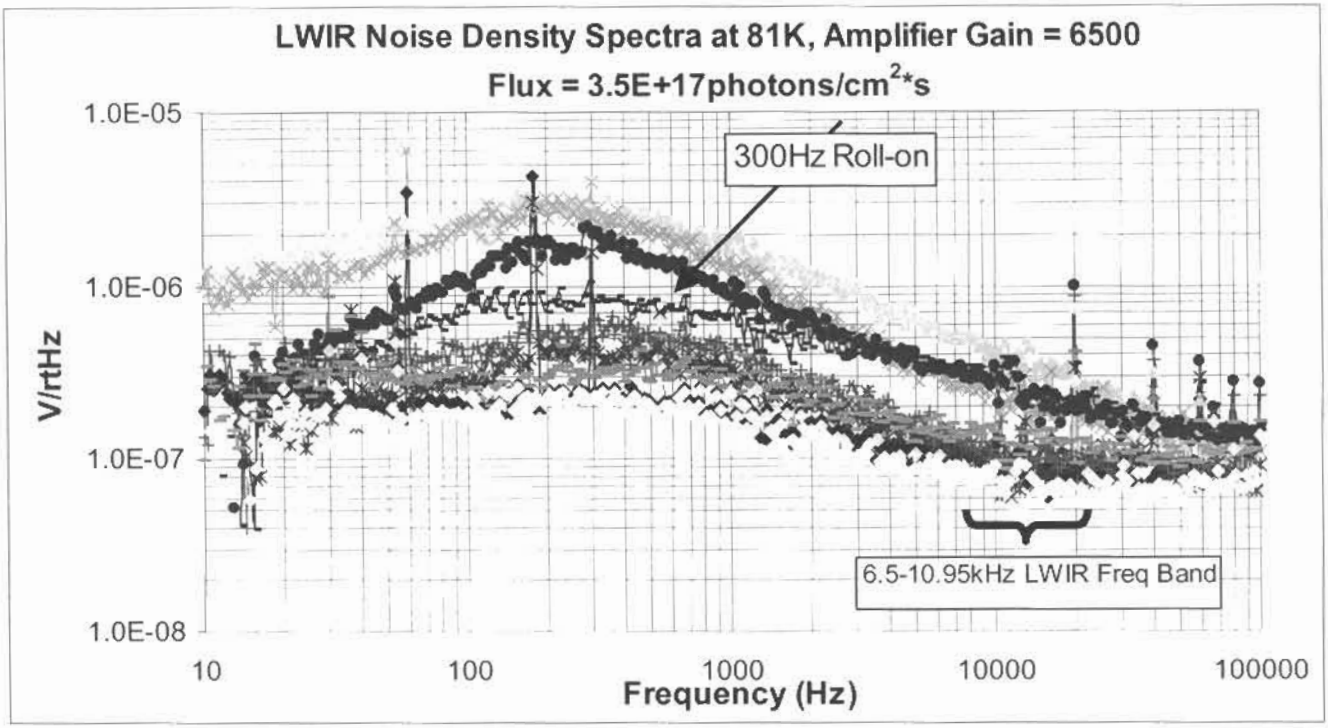

Figure 6 LWIR Noise Density

To calculate D* at the peak wavelength of 14.01μm, the integrated noise within the band of interest is used. The CCA voltage response at average flux and a relative photon response profile are used to generate a spectral response curve. With this data and the integrated noise under the band, a channel's D* can be calculated as per equation 1.

$$D^*(\lambda_p, f) = \frac{\Re * \sqrt{A_{det}} * \sqrt{\Delta f}}{V_n} (Jones)$$

Equation 1.

The D* performance of the EDU2 FPMA diodes are listed in Table 6. For completeness, the maximum D* and the wavelength where this performance was achieved is listed in the table as well.

Table 6

Channel	D* (14.01μm)	Max D*	@ Wavelength (μm)
Channel 1	N/F	N/F	-------
Channel 2	7.18E+09	9.26E+09	13.3
Channel 3	1.55E+10	1.68E+10	13.6
Channel 4	3.25E+10	3.72E+10	13.2
Channel 5	1.62E+10	1.80E+10	13.0
Channel 6	3.45E+10	3.84E+10	13.0
Channel 7	1.20E+10	1.34E+10	13.1
Channel 8	2.31E+10	2.71E+10	13.0
Channel 9	4.87E+10	5.41E+10	13.3

The spectral D* as a function of wavelength is plotted in Figure 7. The average D* at 14.01μm was 2.4E10 +/-1.4E10 Jones.

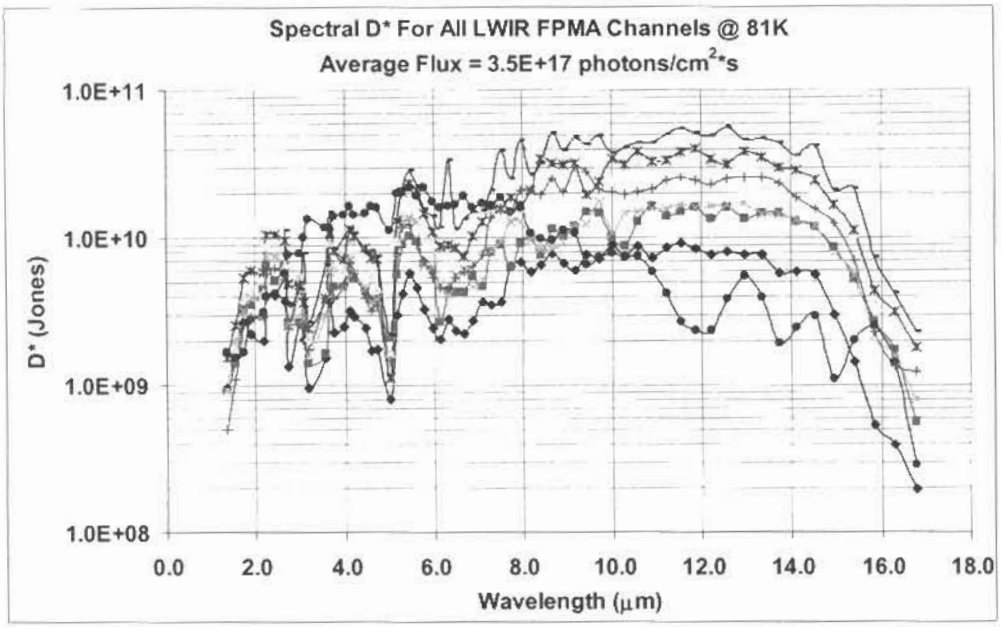

Figure 7 LWIR Spectral D* at 81K and average flux

The LWIR power dissipation measurement required Test Setup C. The current on the 5V DC CCA power supply is measured and multiplied by the 5V supply value to yield the module's total power dissipation. The measured power dissipation was 0.395W. The cooler's power consumption flow down requirement a total of 3.3W for all three modules combined.

6.0 MWIR FPMA Data

The MWIR FPMA was cooled to 98K, biased at –60mV. For the nonlinearity test, the diodes were illuminated with nine flux values between 5.11E16 photons/cm^2*s and 7.36E17 photons/cm^2*s. For the D* calculation and noise measurements in the nominal operating flux of 6.21E17 photons/cm^2*s was used. These flux values were achieved using an Electro-Optical Industries (EOI) Black Body mounted external to the Dewar. The Dewar flux is calibrated using a diode with known quantum efficiency at 98K.

Figure 8 illustrates the linearity of the MWIR FPMA. Each diode is illuminated and the CCA output voltage is recorded for nine different flux values. The outputs are then plotted as a function of flux. Figure 8 shows the deviations from the linear least square fit of the original data as a function of flux. The mean and standard deviation of the nonlinearity the nine channels was 0.04 +/-0.03%.

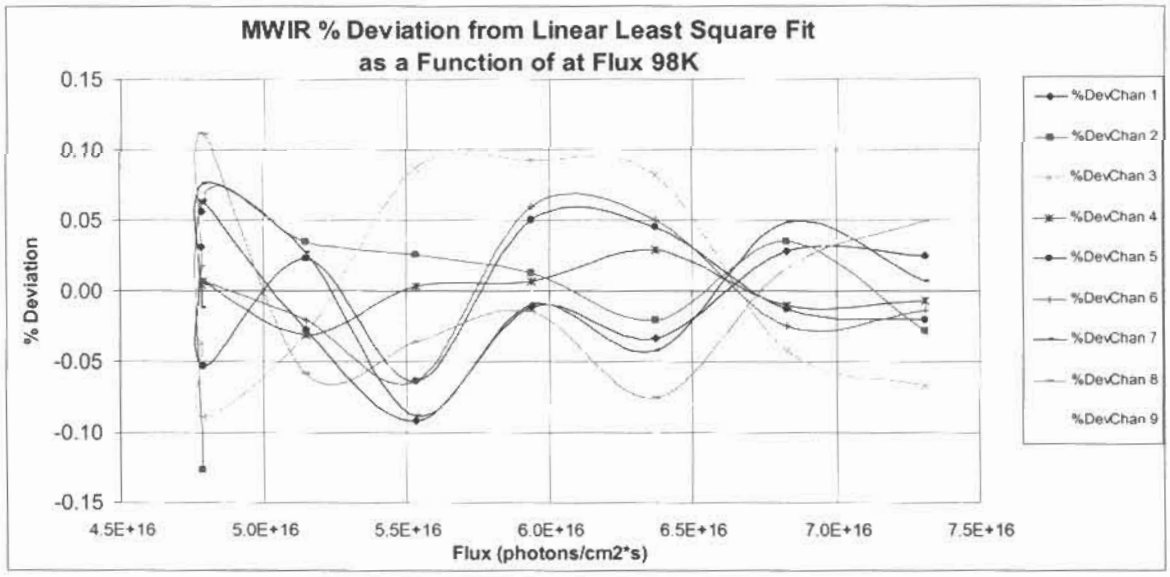

Figure 8 MWIR Nonlinearity

The noise spectral density for all nine channels is plotted in Figure 9. For MWIR, the electrical band of interest is 12.10-17.5kHz. The CCA is A/C coupled for this measurement, which explains the 300Hz roll on of the high pass filter.

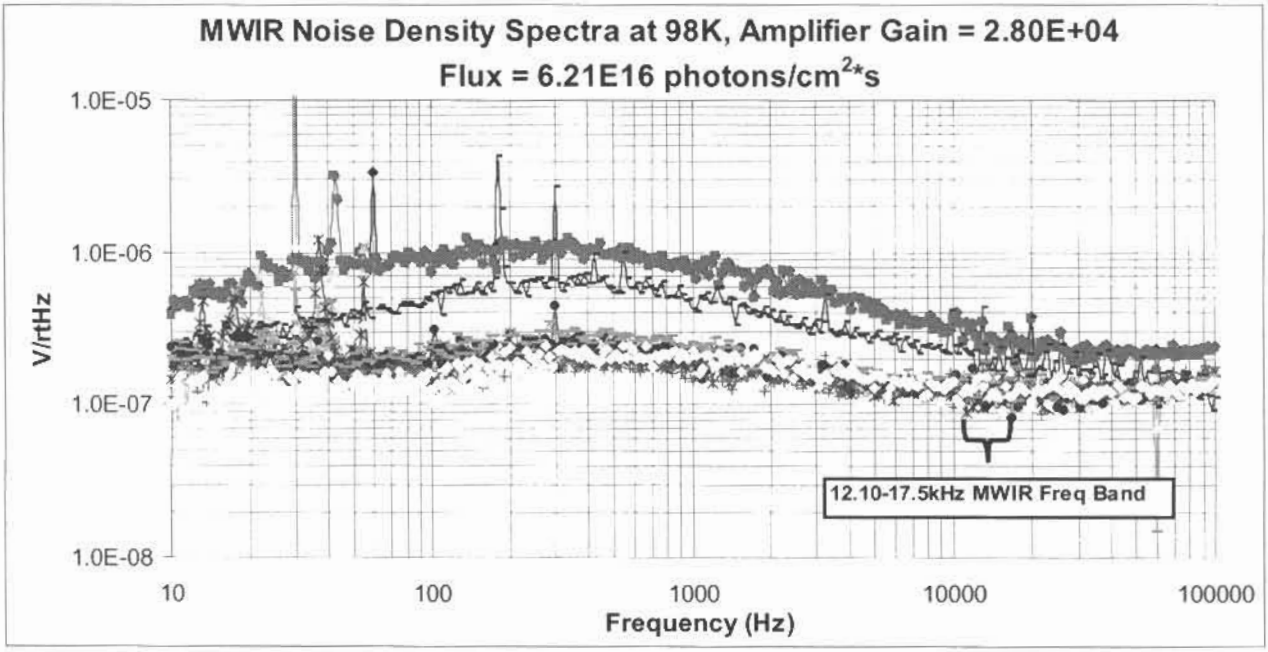

Figure 9 MWIR Noise Spectral Density at 98K and Average Flux

To calculate D* at the peak wavelength of 8.26μm, the integrated noise within the band of interest is used. The CCA voltage response at average flux and a relative photon response profile are used to generate a spectral response curve. With this data and the integrated noise under the band, a channel's D* can be calculated as per equation 1. The LWIR D* performance at 8.26 μm is listed in Table 7.

Table 7

Channel	D*(8.26μm)	Max D*	@ Wavelength (μm)
Channel 1	4.1E+10	4.3E+10	8.02
Channel 2	8.1E+10	8.7E+10	7.99
Channel 3	9.4E+10	1.1E+11	7.91
Channel 4	9.1E+10	1.1E+10	7.95
Channel 5	9.6E+10	1.02E+11	7.99
Channel 6	8.7E+10	9.92E+10	7.84
Channel 7	4.8E+10	5.26E+10	7.95
Channel 8	7.3E+10	7.86E+10	8.10
Channel 9	8.6E+10	9.19E+10	7.99

The spectral D* as a function of wavelength is plotted in Figure 10. The average D* at 8.26μm was 7.7E10 +/- 2.0E10 Jones.

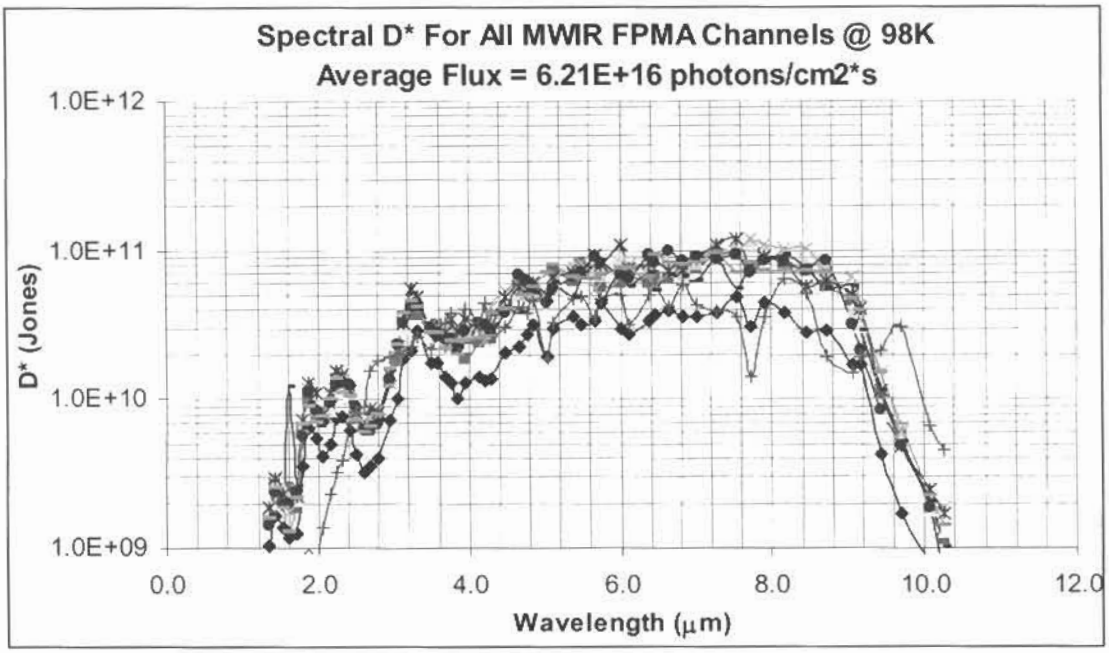

Figure 10 MWIR Spectral D*

6.0 SWIR FPMA Data

The SWIR FPMA was cooled to 98K, biased at –5.0mV. For the nonlinearity test, the diodes were illuminated with nine flux values between 1.49E+15 photons/cm^2*s and 2.12E+15 photons/cm^2*s. For the D* calculation and noise measurements in the nominal operating flux of 1.80E+15 photons/cm^2*s was used. These flux values were achieved using an Electro-Optical Industries (EOI) Black Body mounted external to the Dewar. The Dewar flux is calibrated using a diode with known quantum efficiency at 98K

Figure 11 illustrates the linearity of the FPMA. Each diode is illuminated and the CCA output voltage is recorded for nine different flux values. The outputs are then plotted as a function of flux. Figure 11 illustrates the deviations from the linear least square fit of the original data as a function of flux. The mean and standard deviation of the nonlinearity for the operating channels (excluding channel 1) was 0.07 +/-0.04%.

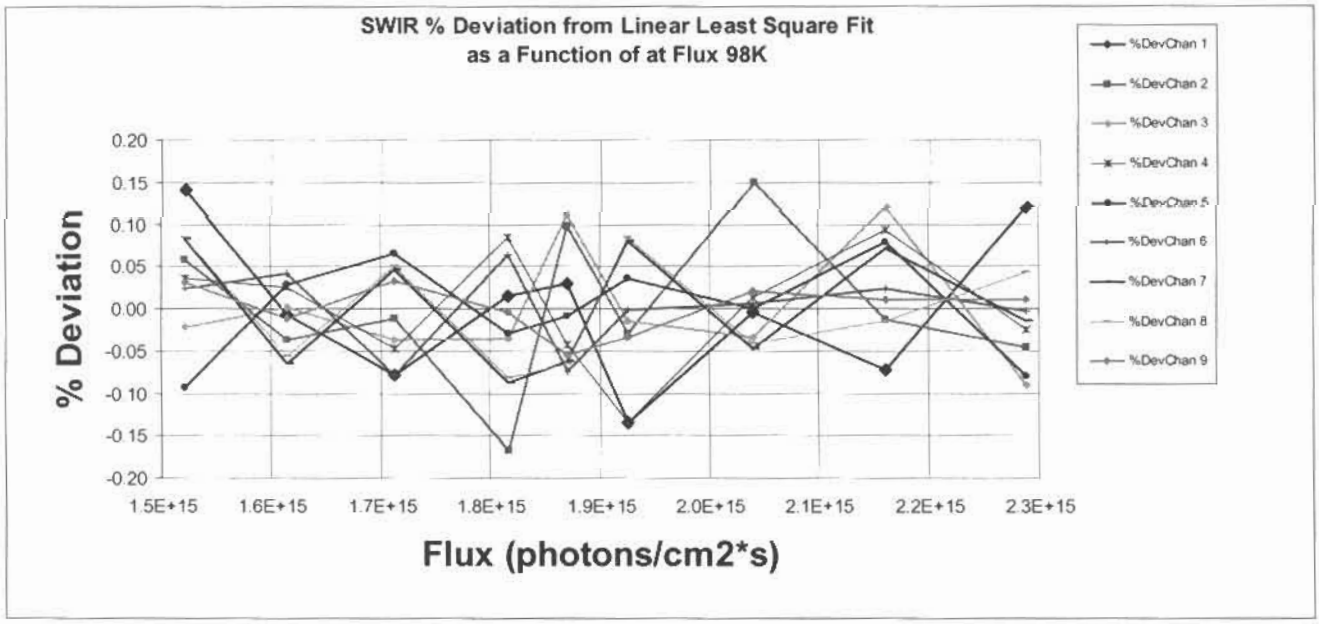

Figure 11 SWIR Nonlinearity

The noise spectral density for all nine channels is plotted in Figure 12. For SWIR, the electrical band of interest is 21.55-25.5kHz. The CCA is A/C coupled for this measurement, which explains the 300Hz roll on of the high pass filter.

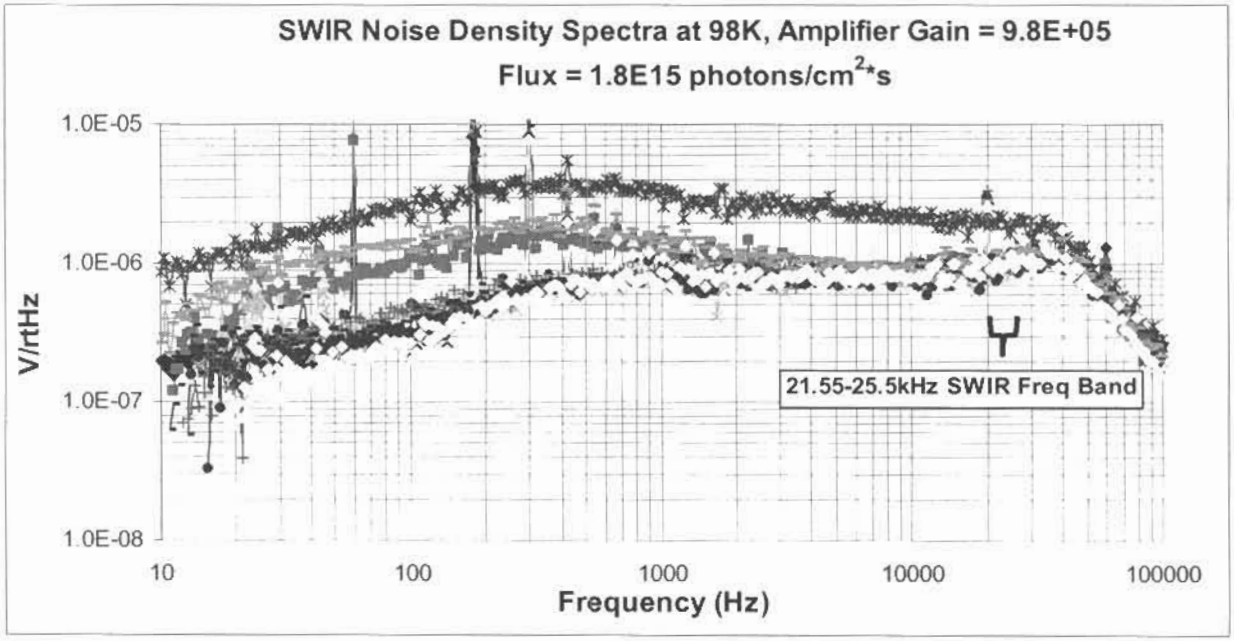

Figure 12 SWIR Noise Spectral Density

To calculate D* at the peak wavelength of 4.64μm, the integrated noise within the band of interest is used. The CCA voltage response at average flux and a relative photon response profile are used to generate a spectral response curve. With this data and the integrated noise under the band, a channel's D* can be calculated as per equation 1. The MWIR D* performance at 4.65μm is listed in Table 8.

Table 8

Channel	D* (4.64μm)	Max D*	@ Wavelength (μm)
Channel 1	2.73E+11	2.78E+11	4.73
Channel 2	2.75E+11	2.83E+11	4.52
Channel 3	3.10E+11	3.16E+11	4.77
Channel 4	1.43E+11	1.47E+11	4.52
Channel 5	3.10E+11	3.16E+11	4.81
Channel 6	3.20E+11	3.23E+11	4.70
Channel 7	3.09E+11	3.14E+11	4.75
Channel 8	2.61E+11	2.66E+11	4.74
Channel 9	2.99E+11	3.07E+11	4.74

The spectral D* as a function of wavelength is plotted in Figure 13. The average D* at 4.64μm was 2.8E11 +/- 5.4E10 Jones.

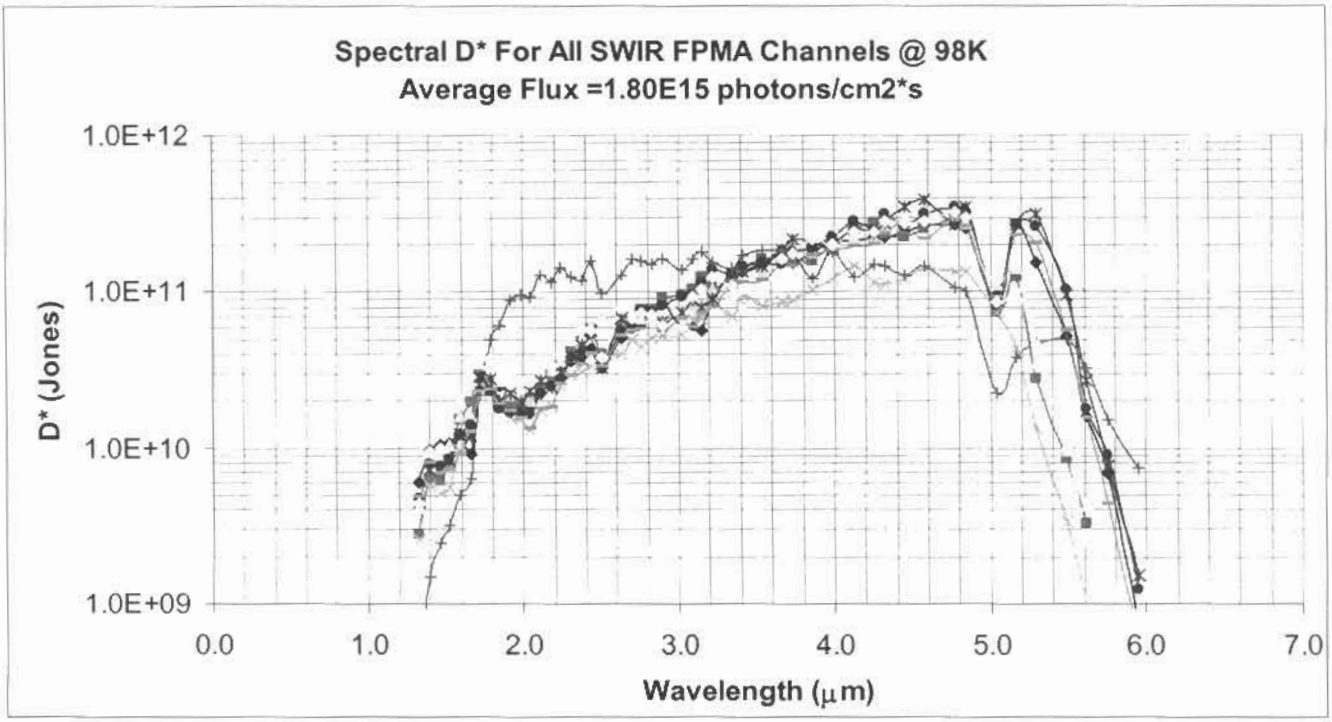

Figure 13 SWIR Spectral D*

7.0 Dynamic Range

The cold and warm electronics were designed such that the CCA Channel outputs would have a nominal range of 0.5V peak-to-peak between minimum and maximum flux. The Dynamic Range of all three modules is listed in Table 8

Table 9

FPMA Dynamic Range	
LWIR	0.731+/- 0.07V
MWIR	0.676 +/- 0.02V
SWIR	0.780 +/- 0.04V

8.0 DPM Ambient Power Dissipation

The power dissipation measurement required Test Setup C. The current on the 5V DC CCA power supply is measured and multiplied by the 5V supply value to yield the module's total power dissipation. The measured power for all three modules is listed in table 9. The cooler's power consumption flow down requirement is a total of 3.3W for all three modules combined. The total power disspation for a all three modules is 1.176 W.

Table 10

Ambient Power Disspation	
LWIR	0.395W
MWIR	0.390W
SWIR	0.391W

9.0 SUMMARY

The testing of the CrIS EDU2 FPMAs yielded data that was typical of the detectors as stand alone devices. The $Hg_{1-x}Cd_xTe$ detectors chosen for the CrIS EDU2 FPMAs have been successfully integrated into a fully functional module platform while accommodating our customer's mechanical and electrical flow-down requirements. Detector-screening parameters developed during the EDU1 phase have been utilized during the EDU2 FPMA build. Data collected during the EDU2 phase validates the diode screening and selection process that will be implemented for EDU3. The data shows the benefits of utilizing PV technology for space-based applications. FPMA linearity performance is 0.16 +/-0.11% for LWIR, 0.04 +/-0.03% for MWIR and 0.07 +/-0.04% for SWIR. FPMA D* performance is 2.4E+10 +/- 1.4E+10 Jones at 14.01μm for LWIR, 7.7E+10 +/-2.0E+10 Jones at 8.26μm for MWIR, and 2.8E+11 +/-5.4E+10 Jones at 4.64μm for SWIR. Changes to detector architecture for LWIR will enhance operability and improve detector yields in the future.

10.0 REFERENCES

1. J.M. Arias, J.G. Pasko, M. Zandian, L.J. Kozlowski and R.E. DeWames, *Optical Engineering* **33**, 1422(1994).
2. J.M. Arias, J.G. Pasko, M. Zandian, J. Bajaj, L.J. Kozlowski, R.E. DeWames, and W.E. Tennant, "Proceedings of SPIE Symposia on Producibility of II-VI Materials and Devices", Vol. 2228, p. 210 (1994).
3. J. Bajaj, J.M. Arias, M. Zandian, J.G. Pasko, L.J. Kozlowski, R.E. DeWames, W.E. Tennant, *J. Electron. Mater.* **24**, 1067 (1995).
4. J. Bajaj, J.M. Arias, M. Zandian, J.G. Pasko, L.J. Kozlowski, R.E. DeWames and W.E. Tennant, *J. Electron. Mater.* **25**, 1394 (1996).
5. D.D. Edwall, M. Zandian, A.C. Chen, and J. M. Arias, *J. Electron. Mater.* **26**, 493 (1997).
6. A.I. D'Souza, L.C. Dawson, E.J. Anderson, A.D. Markum, W.E. Tennant, L.O. Bubulac, M. Zandian, J.G. Pasko, W.V. McLevige, D.D. Edwall, *J. Electron. Mater.* 26, 656 (1997).